Experimental demonstration of a tomographic five-dimensional phase-space reconstruction

S. Jaster-Merz,[1,*] R. W. Assmann,[1,†] J. Beinortaitė,[1] J. Björklund Svensson,[1,‡] R. Brinkmann,[1] F. Burkart,[1] P. Craievich,[2] H. Dinter,[1] P. González Caminal,[1,§] W. Hillert,[3] A. L. Kanekar,[1] M. Kellermeier,[1] W. Kuropka,[1] F. Mayet,[1] J. Osterhoff,[1,‖] B. Stacey,[1] M. Stanitzki,[1] T. Vinatier,[1] S. Wesch,[1] and R. D'Arcy[1,¶]

[1]*Deutsches Elektronen-Synchrotron DESY, Hamburg, Germany*

[2]*Paul Scherrer Institut, Villigen, Switzerland*

[3]*Department of Physics, Universität Hamburg, Hamburg, Germany*

(Received 20 May 2025; accepted 14 October 2025; published 24 November 2025)

Detailed knowledge of particle-beam properties is of great importance to understand and push the performance of existing and next-generation particle accelerators. We recently proposed a phase-space tomography method to reconstruct the five-dimensional (5D) phase space, i.e., the charge density distribution in all three spatial directions and the two transverse momenta. Here, we present the first experimental demonstration of the method at the FLASHForward facility at DESY. This includes the reconstruction of the 5D phase-space distribution of a GeV-class electron bunch, the use of this measured phase space to create a particle distribution for simulations, and the extraction of the transverse 4D slice emittance.

DOI: 10.1103/m4wh-mhdm

I. INTRODUCTION

Particle accelerators are highly complex and multivariate machines that are required to produce beams with percent- to subpermille-level stability at highly specialized working points with limited diagnostics. The generation of these beams is especially difficult for applications that require excellent phase-space quality such as advanced ultrahigh-gradient accelerators [1–10] or free-electron lasers [11–18], and their complex operation modes (e.g., twin bunches or two-color lasing [19–22]).

To characterize these electron beams, methods focusing on the reconstruction of statistical beam parameters or two-dimensional (2D) projections of the full phase space [23–28] are routinely used. For higher-dimensional structures, especially when correlations between the transverse and longitudinal phase spaces are present, the above-mentioned techniques are insufficient. Tomographic methods have been successfully applied to these cases, e.g., for measuring the time-resolved transverse phase-space distribution [29], the full 4D transverse phase space [30–33], and the full 3D spatial distribution [34–37].

The development of the polarizable X-band transverse-deflection structure (PolariX TDS) [37–39] by a collaboration of scientists from CERN, PSI, and DESY enables the extension of these existing diagnostics abilities [34,37,40] to include streaking of the bunch in any transverse direction. Based on this capability, we recently proposed a method that extends the existing tomographic methods by an extra dimension and reconstructs the full 5D phase-space density of bunches [41], i.e., the transverse positions (x, y) and divergences (x', y') as well as the time coordinate t. This technique combines a quadrupole-based 4D transverse tomography [30] in normalized phase space with the streaking of the bunch along various directions by the PolariX TDS. Simulation studies of the 5D tomography method have shown the successful reconstruction of the 5D phase space of complex beam distributions [41].

Other methods have been studied to obtain higher-dimensional information. For subrelativistic beams, a combination of horizontal and vertical slit masks can be used and has been benchmarked with a 2.5 MeV H^- beam for 5D [42] and 6D [43] reconstructions. Also machine-learning-based methods can be applied, which predict the phase-space projections up to the full 6D particle distribution [44–51] in potentially short measurement periods at a cost of a less predictable resolution in the obtained features and charge density.

In this work, we focus on the use of tomographic methods that are based on direct measurements of all relevant phase-space projections, thereby providing knowledge of the obtained resolution in all reconstructed dimensions. We present the first 5D tomographic reconstruction of an electron bunch as well as self-consistent checks to validate the results. We show that the method resolves previously hidden correlations between all the transverse planes and time coordinate and in addition allows the 4D slice emittance to be extracted. Furthermore, by propagating the reconstructed 5D distribution along the beamline, possibilities open up for performing highly accurate simulation studies to understand and optimize

*Contact author: sonja.jaster-merz@desy.de

†Present address: GSI Helmholtzzentrum für Schwerionenforschung GmbH, Darmstadt, Germany.

‡Present address: Lund University, Lund, Sweden.

§Present address: ATG Science & Technology S.L., Barcelona, Spain.

‖Present address: Lawrence Berkeley National Laboratory, Berkeley, California 94720, USA.

¶Present address: Oxford University, Oxford, United Kingdom.

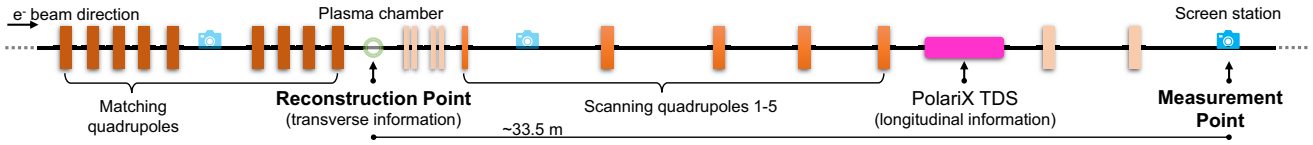

FIG. 1. The FLASHForward beamline section used for the 5D tomography measurement. The transverse phase space is reconstructed at the location labeled as the reconstruction point. The reconstruction of the time information is obtained at the PolariX TDS. The screen images for the tomography were recorded at the measurement point. Beamline elements that were not used for the measurement are displayed in a fainter color.

the accelerator performance or to benchmark the results of simulation codes.

II. EXPERIMENTAL DEMONSTRATION

A. Measurement setup

The measurement campaign was performed at the FLASHForward facility [52], which is dedicated to beam-driven plasma-acceleration experiments. It uses the high-quality and stable electron bunches provided by the free-electron laser in Hamburg (FLASH) linear accelerator [11,53,54]. A sketch of the relevant beamline section is shown in Fig. 1. To record the beam images, a screen station downstream of the PolariX TDS was used with Scheimpflug optics, a cerium-doped gadolinium aluminum gallium garnet scintillating screen, and a nominal resolution of 10 µm [55]. Nine quadrupoles were operated to set the beam optics [56] to $\beta_x = \beta_y = 10\,\mathrm{m}$ and $\alpha_x = \alpha_y = 0$ at the reconstruction point. The 5D tomography method [41] simultaneously controls the horizontal and vertical phase advances between the reconstruction point and measurement point. These phase advances were varied using five quadrupoles covering a range of 180° in ten steps in both transverse planes. The required quadrupole strengths were determined in simulations. For each phase-advance combination, the beam was streaked using the PolariX TDS at ten transverse angles covering approximately 180°. This resulted in a total of 1000 planned scan steps. All quadrupoles between the TDS and measurement screen were switched off as identical beam optics in all transverse directions between these points are required for the tomographic reconstruction of the charge density [35]. The shear parameter, relating the measured transverse coordinate along the streaking direction at the measurement point to the longitudinal position within the bunch at the TDS location, was measured for all streaking angles by means of a radio-frequency (RF) phase scan. The PolariX amplitude was set to the maximum of the available RF power at an average value of 4.5 MW ± 0.3 MW resulting in an average shear parameter of 18.7 ± 2.5. The beta function at the measurement point was kept approximately at $\beta_x = \beta_y = 10\,\mathrm{m}$ to obtain a near-constant longitudinal resolution in the tens-of-femtosecond range while maintaining an achievable optics setup for the beamline.

For the 5D phase-space-tomography measurement, the quadrupoles were cycled between scan points whenever their ramping direction was changed to prevent hysteresis effects. For each scan point, ten screen images with beam as well as ten background images were recorded. In addition, screen images of the unstreaked beam were collected. During the experiment, 960 out of 1000 scan points were recorded successfully in 28 h. Charge and compression feedbacks were enabled to obtain a stable beam with rms variations below 1% for the charge and below 8% for the bunch length over the entire measurement. The measurement was conducted at a beam energy of 1.09 GeV ± 0.01 GeV and with an average beam charge of 297 pC ± 2 pC.

B. Five-dimensional tomographic reconstruction

The 5D tomographic reconstruction procedure is described in detail in Ref. [41]. A Python scikit-image implementation of the SART (simultaneous algebraic reconstruction technique) algorithm [57,58] was used with two iterations. In a first step, the 3D charge-density distribution was reconstructed [34] at the measurement location for each phase-advance combination. This distribution was then converted into normalized coordinates using the Courant-Snyder parameters [56] at this location obtained from simulations. For each time slice of the bunch, the transverse distributions of all phase-advance settings were combined and the 4D phase space was reconstructed using a method similar to the one presented in Ref. [30]. Finally, by joining all time slices the 5D distribution $(x_N, x'_N, y_N, y'_N, t)$ was obtained. The time information was reconstructed at the location of the PolariX TDS using 72 slices of 20 fs duration, with the duration approximately corresponding to the average longitudinal resolution of 19 fs ± 5 fs. The transverse information was reconstructed upstream of the five scanning quadrupoles (see Fig. 1) with 301 bins in each transverse direction in a range of $\pm 5 \times 10^{-4}\,\mathrm{m}/\sqrt{\mathrm{m}}$ corresponding to an approximate bin size of the assumed 10 µm screen resolution. A constant beam charge was assumed in all tomographic reconstructions. The tomographic reconstruction was performed in approximately 7 h on an AMD EPYC 75F3 node.

The projection of the reconstructed 5D phase space onto the ten 2D planes is shown in Fig. 2, which constitutes the first direct and simultaneous measurements of these projections for ultrarelativistic electron beams. Nonlinear correlations between all transverse planes and the time coordinate are visible. The projected normalized transverse phase spaces deviate from the matched circular case and exhibit non-Gaussian structures, which are visible especially in the (x'_N, y'_N) and (y_N, y'_N) planes. These features mainly stem from varying centroid and momentum offsets along the bunch. Such correlations can appear in linear accelerators and can be caused by collective effects, such as space charge and coherent synchrotron radiation (CSR) occurring, e.g., during the compression of the bunch [59,60]. In particular, the correlations in the (x_N, t) plane are expected to originate

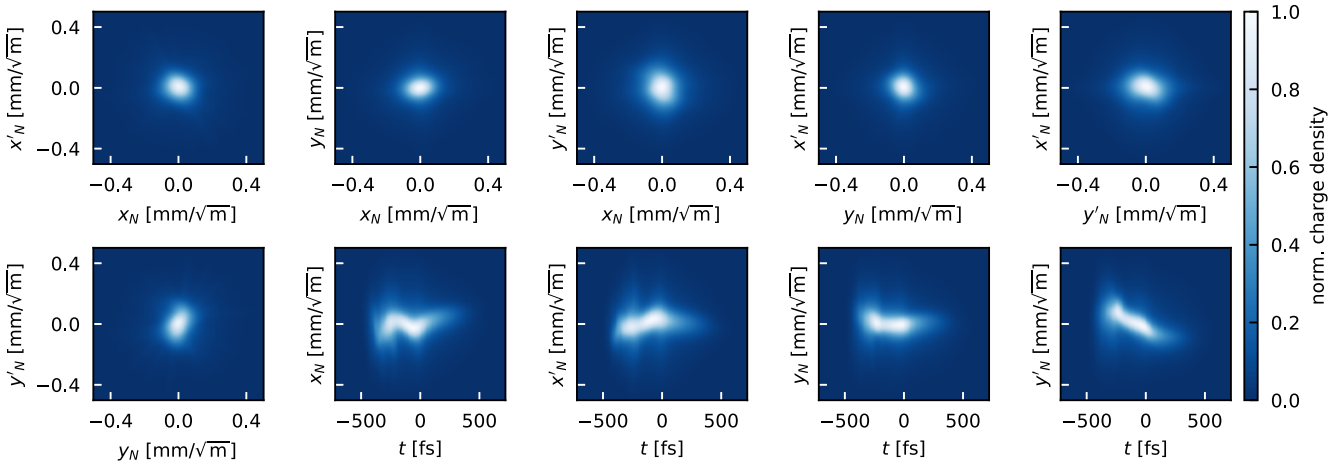

FIG. 2. 2D projections of the reconstructed 5D phase-space distribution normalized to their maximum value. The transverse projections are shown in normalized phase space. The head of the bunch is toward negative time values.

from CSR effects induced in the two horizontal bunch compressor chicanes located upstream in the FLASH linac, as qualitatively similar features have also been observed in previous simulation studies [34,36]. The correlations in the (y'_N, t) phase space cannot be explained by these CSR effects. We believe that these correlations are caused by the remaining vertical dispersion in the beamline that, in combination with the induced energy chirp during bunch compression, would lead to correlations between the vertical planes and the time coordinate. An optimization of the observed correlations was beyond the scope of this proof-of-principle demonstration but is now possible due to the ability of the 5D tomography method to unveil these effects.

In addition to the 2D projections, the projection onto the 3D (x'_N, y'_N, t) phase space is shown in Fig. 3, highlighting three transverse slices along the bunch and the ability of the method to provide a time-resolved measurement of these less conventional transverse phase spaces. The aforementioned features and nonlinear correlations, as well as momentum offsets, are also visible here. Furthermore, the reconstruction can be used to create a particle distribution with a significant number of macroparticles, in the presented case 5 million. The distribution is generated slicewise by randomly creating particles in accordance with the probability distribution of the reconstructed phase space. Only probability values larger than 5% of the maximum value of each slice are appropriately populated. This threshold has been found to be a good balance between removing noise introduced by the tomographic reconstruction, typically occurring far off-axis and arising due to the finite amount of projection angles [37], and preserving the features of the reconstructed distribution. The obtained distribution is used to calculate the beam covariance matrix Σ^{4D} for all slices containing at least 10 000 particles and extract the slice beam parameters shown in Fig. 4 like the transverse Courant-Snyder parameters, normalized emittances ϵ_x^n and ϵ_y^n, and the current profile. Variations of these parameters along the bunch are visible as well as a mismatch to the design values of $\beta = 10\,\mathrm{m}$ and $\alpha = 0$. In addition, the sliced 4D emittance $\epsilon^{4D} = \sqrt{\det \Sigma^{4D}}$ is extracted. It is a measure of the minimum transverse emittances that can be reached in the case that all correlations between the planes are eliminated [61]. As the lasing performance of FELs and the luminosity of colliders depend on the transverse emittances [62,63], having the ability to now measure and in the future correct for correlations is highly beneficial. The measured sliced 4D emittance is shown in Fig. 4(d) and compared to a multiplication of the two transverse emittances $\epsilon^{4D}_{\mathrm{approx.}} = \epsilon_x \epsilon_y$, which are accessible with conventional PolariX TDS measurements. The average relative discrepancy is 5% with a minimum of 1% at around −170 fs. The measurement therefore indicates that only minor correlations between the transverse planes are present, which are minimal at the core part of the bunch.

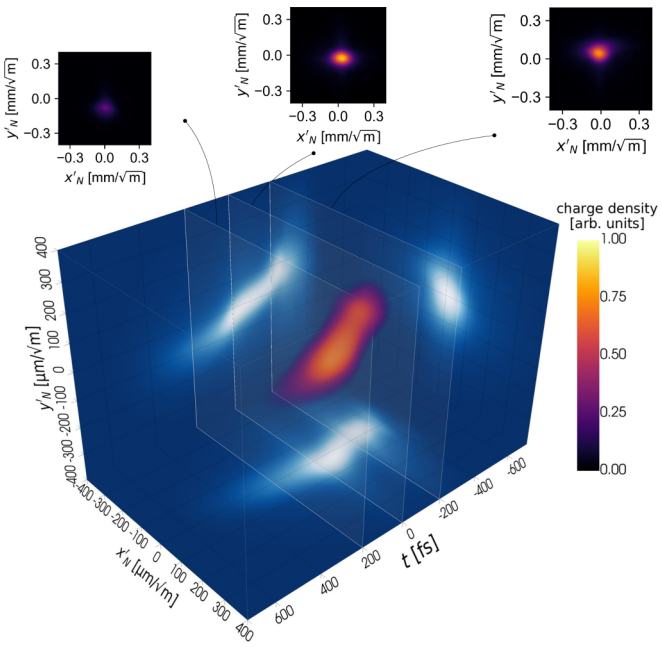

FIG. 3. Rendering of the reconstructed 5D phase-space distribution projected onto the (x'_N, y'_N, t) phase space. The projection is normalized to the maximum value of the charge density. In addition, the 2D projections are displayed in blue color and exemplarily three transverse slices are included.

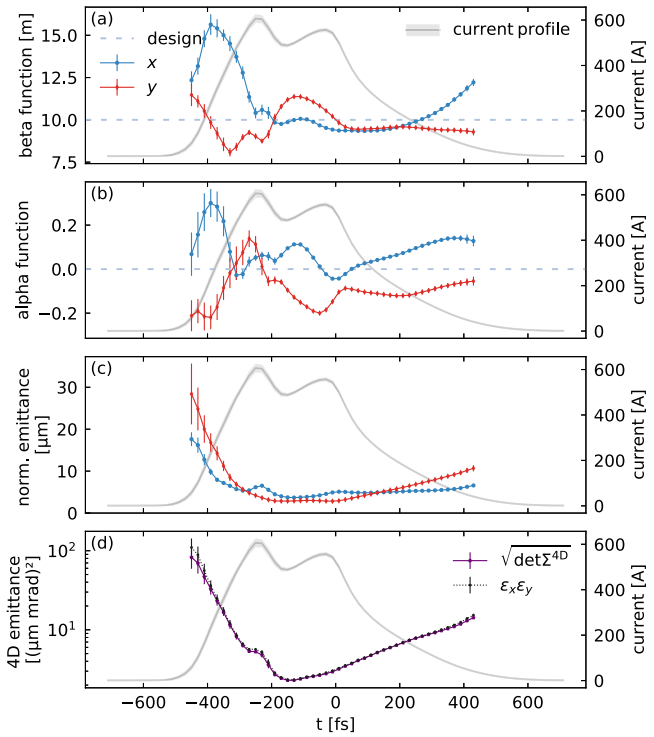

FIG. 4. Reconstructed current profile, (a) beta functions, (b) alpha functions, and (c) sliced normalized transverse emittances for both transverse planes obtained from the 5D charge density. (d) The sliced 4D emittance is compared to the value obtained when multiplying the two transverse emittances. Only slices that contain at least 10 000 particles (0.2% of the total charge) are analyzed and the error bars are obtained from 100 reconstructions, where the shear parameter of each streaking angle is randomly sampled from a Gaussian distribution with a one-sigma measurement uncertainty.

III. VALIDATION

The tomographic reconstruction is validated using two approaches. First, the beam parameters obtained from the tomographic reconstruction are compared to lower-dimensional complementary measurements listed in Table I. To obtain the normalized transverse rms emittances and Courant-Snyder parameters, a multiquadrupole scan analysis is performed using the unstreaked beam images. The uncertainties are obtained from statistical fluctuation from ten different datasets recorded throughout the 5D tomography measurement. The uncertainty on the tomographic reconstruction is estimated by performing 100 reconstructions using the Python library Optimas [64], where the shear parameter of each streaking angle is randomly sampled from a Gaussian distribution and a one-sigma measurement uncertainty is applied. In addition, errors on the reconstruction due to an energy uncertainty (a 1% energy error results in a 5% emittance error), an energy spread within the distribution (a projected rms energy spread of 1% consisting of a linear energy chirp and an uncorrelated rms energy spread of 0.1% result in a 2% emittance error), and the finite number of projection angles (ten angles per plane result in an overestimation of the emittance by up to 13%) are expected. While these measurement errors are expected to apply equally to both transverse planes, we suspect that the larger discrepancy in the vertical emittance can be explained by an incomplete dataset of the last vertical phase-advance scan (and hence a reduced number of recorded projections compared to the horizontal plane) resulting in an increased measurement uncertainty in this plane. The discrepancies in the alpha functions cannot be explained by the expected measurement uncertainties of the two methods. The beta functions and horizontal emittance agree well between the two methods within the estimated uncertainties. The bunch duration is determined using the screen images of the streaked beam at both zero crossings. Following Refs. [65,66], linear correlations within the bunch are taken into account resulting in an rms bunch duration of 194 fs ± 16 fs, which is in excellent agreement with the result of 199^{+8}_{-7} fs obtained from the tomography.

TABLE I. Reconstructed beam parameters.

Parameters	Units	Tomography	Quadrupole scan
ϵ_x^n	μm	6.63 ± 0.10	6.22 ± 0.68
ϵ_y^n	μm	8.25 ± 0.20	6.69 ± 0.62
α_x	–	0.09 ± 0.00	0.37 ± 0.08
α_y	–	−0.28 ± 0.01	0.05 ± 0.14
β_x	m	10.75 ± 0.04	11.74 ± 1.50
β_y	m	7.44 ± 0.05	7.04 ± 0.61
σ_t	fs	199^{+8}_{-7}	194 ± 16[a]

[a]Obtained from streaked screen images at both zero crossings.

Second, the obtained particle distribution from the reconstructed 5D phase space is tracked from the reconstruction point to the measurement point for all beamline settings that were used in the measurement. The obtained simulated screen images of the distribution are then compared to the measured ones. This comparison is done in the (υ, t) coordinates, where υ is the transverse plane perpendicular to the streaking direction and t is the time axis obtained by scaling the streaking plane with the shear parameter. As a measure of deviation between the reconstructed and measured projections, the deviations between the centroid position of each time slice normalized to the rms spread of the measured distribution are determined, and the average weighted by the slice charge is calculated. Only slices that contain more than 0.5% of the total charge are taken into account. The average relative discrepancy for all recorded projections is 32% ± 15%. A visual comparison of the measured and tracked screen images shows that for most projections a qualitatively accurate reconstruction of the beam shape is obtained, as can be seen in a subset of the data shown in Fig. 5. The main discrepancy between the measured and tracked projections is expected to stem from a blurring and loss of small beam features, which are especially sensitive to uncertainties in the shear parameter, as well as small changes in the distribution over the measurement time.

Overall, the two validations indicate a reasonable agreement of the reconstructed 5D distribution with lower-dimensional complementary measurements and thereby support the experimental usability of the 5D tomography method.

IV. CONCLUSION

In this work, we presented the first tomographic reconstruction of the 5D phase space of an electron beam and the

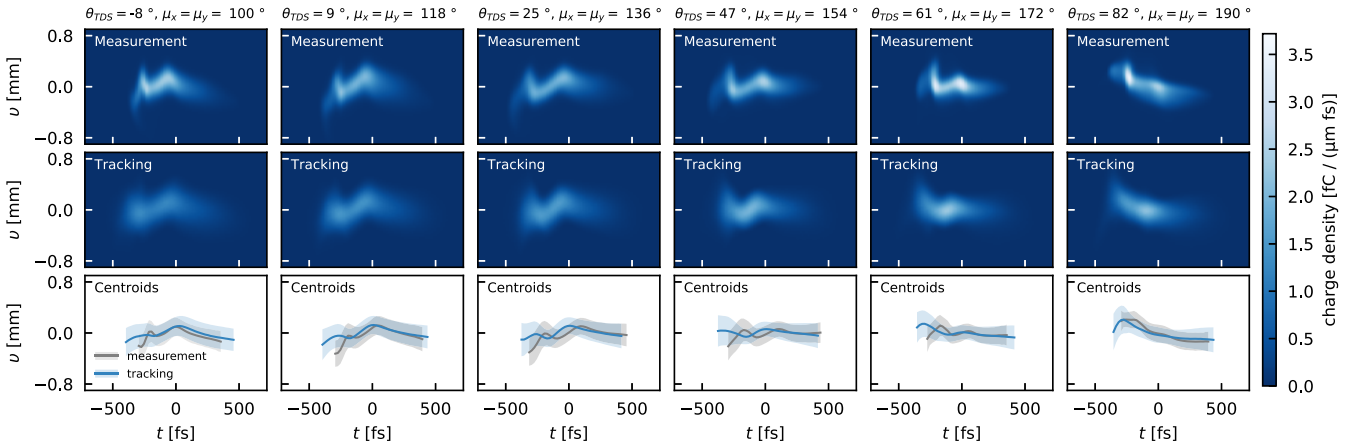

FIG. 5. Comparison of the measured screen images (top) to the tracked distribution (middle) for various phase advances μ_x, μ_y. The screen images are rotated by the streaking angle θ_{TDS} and the projection in streaking direction is converted to the time axis. The coordinate υ denotes the transverse plane of the bunch perpendicular to the streaking plane. The bottom row shows the centroid positions and rms spread for each time slice containing more than 0.5% of the total charge.

validation of the result against lower-dimensional projections. The 2D projections of the reconstructed phase space show correlations between the transverse and longitudinal planes that were not detectable with previous diagnostic methods. Furthermore, the tomographic reconstruction facilitated the first sliced 4D emittance measurement at a free-electron laser. While the reconstructed bunch was not optimized for FEL or plasma operation, both applications can benefit from the presented measurement method as undesired correlations that either degrade the transverse emittances (and hence the lasing performance of FELs) or drive instabilities in beam-driven plasma accelerators [2,67,68] can be identified and minimized. Furthermore, conversion of the reconstructed phase space into a particle distribution enables highly realistic simulations of the beamline with the potential to better understand and improve its performance. A future combination of such a 5D tomography with an additional longitudinal phase-space measurement would provide a quasicomplete characterization of electron beams. These results can additionally be used to benchmark other diagnostic methods, e.g., based on machine learning [51].

To increase the viability of the measurement, a reduction of the measurement time is strongly desired. During the measurement campaign, we could already show that an optimized operation of the PolariX RF amplitude while changing the streaking angle reduces the measurement time by up to 30%. The remaining dominant factor was the cycling of the quadrupoles. If the measurement is modified in such a way that no cycling is needed, the measurement time can be reduced substantially. Proof-of-principle tests in this direction at the accelerator research experiment at SINBAD (ARES) accelerator [69] have in fact been shown to reduce the measurement time by up to 80% [33]. Also the reconstruction time can be reduced further. By adapting the reconstructed transverse region of interest, the reconstruction can be performed within 1 h while keeping the same resolution. Further reduction in time is possible by reducing the number of reconstructed bins (e.g., to less than 4 min for 51 bins per transverse plane). Finally, as the presented method does not depend on a specific reconstruction algorithm (here SART), the combination with machine-learning-assisted reconstruction methods [48–51,70] or tomography algorithms based on particle sampling [26,71] could be explored to reduce the measurement and reconstruction time. The extension of the presented method to full 6D is part of future work and could include the combination of the tomography with additional longitudinal phase-space and energy measurements, or the implementation of a full tomography-based solution including dispersive measurements in all transverse directions.

ACKNOWLEDGMENTS

We would like to thank S. Schreiber and the scientific committee at FLASH for supporting this study and providing this beamtime, M. Vogt for the support on the PolariX structures, and the FLASH operators for their support during the beamtime. We thank the technical groups for their support, especially R. Jonas for helpful advice on the operation of the PolariX phase shifter. Furthermore, we thank A. Wolski for helpful discussions on optimizing the beamline for the tomographic measurement, A. Ferran Pousa for helpful discussions on the data analysis and the support on the optimas library, and B. Beutner for the helpful discussions on the results. This research was supported in part through the Maxwell computational resources operated at DESY, Hamburg, Germany. We acknowledge support from DESY Hamburg, Germany, a member of the Helmholtz Association HGF.

S.J.-M., R.W.A., R.B., F.B., W.H., M.S., and T.V. conceptualized the work and proposed the experiment. S.J.-M., F.B., P.G.C., and R.D. planned the experiment. S.J.-M., P.G.C., F.M., and S.W. conducted preparatory work for the experiment. S.J.-M., J.B., J.B.S., F.B., P.C., R.D., H.D., P.G.C., A.L.K., M.K., W.K., F.M., B.S., T.V., and S.W. conducted the experiment. S.J.-M. performed the data analysis and wrote the manuscript. J.B., J.B.S., F.B., P.G.C., R.D., H.D., M.K., W.K., F.M., T.V., and S.W. contributed to the manuscript. Everybody read the manuscript and contributed to discussions of the results.

DATA AVAILABILITY

The data that support the findings of this article are not publicly available upon publication because it is not technically feasible and/or the cost of preparing, depositing, and hosting the data would be prohibitive within the terms of this research project. The data are available from the authors upon reasonable request.

[1] P. Chen *et al.*, Acceleration of electrons by the interaction of a bunched electron beam with a plasma, Phys. Rev. Lett. **54**, 693 (1985).

[2] D. H. Whittum *et al.*, Electron-hose instability in the ion-focused regime, Phys. Rev. Lett. **67**, 991 (1991).

[3] M. Galletti *et al.*, Stable operation of a free-electron laser driven by a plasma accelerator, Phys. Rev. Lett. **129**, 234801 (2022).

[4] C. Joshi *et al.*, Plasma wakefield acceleration experiments at FACET II, Plasma Phys. Controlled Fusion **60**, 034001 (2018).

[5] E. o. Adli, Acceleration of electrons in the plasma wakefield of a proton bunch, Nature (London) **561**, 363 (2018).

[6] I. Blumenfeld *et al.*, Energy doubling of 42 GeV electrons in a metre-scale plasma wakefield accelerator, Nature (London) **445**, 741 (2007).

[7] M. Litos *et al.*, High-efficiency acceleration of an electron beam in a plasma wakefield accelerator, Nature (London) **515**, 92 (2014).

[8] M. Ferrario *et al.*, SPARC_LAB present and future, Nucl. Instrum. Methods Phys. Res. Sect. B **309**, 183 (2013).

[9] R. Pompili *et al.*, Free-electron lasing with compact beam-driven plasma wakefield accelerator, Nature (London) **605**, 659 (2022).

[10] B. Hidding *et al.*, Progress in hybrid plasma wakefield acceleration, Photonics **10**, 99 (2023).

[11] J. Rossbach *et al.*, 10 years of pioneering X-ray science at the Free-Electron Laser FLASH at DESY, Phys. Rep. **808**, 1 (2019).

[12] R. Abela *et al.*, *XFEL: The European X-ray Free-Electron Laser: Technical Design Report* (DESY, Hamburg, 2006), pp. 1–646.

[13] P. Emma *et al.*, First lasing and operation of an ångstrom-wavelength free-electron laser, Nat. Photon. **4**, 641 (2010).

[14] T. Ishikawa *et al.*, A compact X-ray free-electron laser emitting in the sub-ångström region, Nat. Photon. **6**, 540 (2012).

[15] L. Giannessi *et al.*, Status and perspectives of the FERMI FEL facility (2019), in *Proceedings of FEL'19*, *Free Electron Laser Conference No. 39* (JACoW Publishing, Geneva, Switzerland, 2019), pp. 742–745.

[16] H.-S. Kang *et al.*, Hard X-ray free-electron laser with femtosecond-scale timing jitter, Nat. Photon. **11**, 708 (2017).

[17] E. Prat *et al.*, A compact and cost-effective hard X-ray free-electron laser driven by a high-brightness and low-energy electron beam, Nat. Photon. **14**, 748 (2020).

[18] B. Liu *et al.*, The SXFEL upgrade: From test facility to user facility, Appl. Sci. **12**, 176 (2022).

[19] A. Marinelli *et al.*, High-intensity double-pulse X-ray free-electron laser, Nat. Commun. **6**, 6369 (2015).

[20] E. Schneidmiller and I. Zagorodnov, Two-bunch seeding of soft x-ray free electron lasers, Phys. Rev. Accel. Beams **27**, 110703 (2024).

[21] E. Ferrari *et al.*, Widely tunable two-colour seeded free-electron laser source for resonant-pump resonant-probe magnetic scattering, Nat. Commun. **7**, 10343 (2016).

[22] E. Prat *et al.*, Widely tunable two-color x-ray free-electron laser pulses, Phys. Rev. Res. **4**, L022025 (2022).

[23] C. McKee *et al.*, Phase space tomography of relativistic electron beams, Nucl. Instrum. Methods Phys. Res. Sect. A **358**, 264 (1995).

[24] D. Stratakis *et al.*, Tomography as a diagnostic tool for phase space mapping of intense particle beams, Phys. Rev. ST Accel. Beams **9**, 112801 (2006).

[25] V. Yakimenko *et al.*, Electron beam phase-space measurement using a high-precision tomography technique, Phys. Rev. ST Accel. Beams **6**, 122801 (2003).

[26] B. Hermann *et al.*, Electron beam transverse phase space tomography using nanofabricated wire scanners with submicrometer resolution, Phys. Rev. Accel. Beams **24**, 022802 (2021).

[27] D. Dowell *et al.*, Longitudinal emittance measurements at the SLAC gun test facility, Nucl. Instrum. Methods Phys. Res. Sect. A **507**, 331 (2003).

[28] D. Malyutin *et al.*, Longitudinal phase space tomography using a booster cavity at PITZ, Nucl. Instrum. Methods Phys. Res. Sect. A **871**, 105 (2017).

[29] M. Röhrs, C. Gerth, H. Schlarb, B. Schmidt, and P. Schmüser, Time-resolved electron beam phase space tomography at a soft x-ray free-electron laser, Phys. Rev. ST Accel. Beams **12**, 050704 (2009).

[30] K. Hock *et al.*, Tomographic reconstruction of the full 4D transverse phase space, Nucl. Instrum. Methods Phys. Res. Sect. A **726**, 8 (2013).

[31] A. Wolski *et al.*, Transverse phase space characterization in an accelerator test facility, Phys. Rev. Accel. Beams **23**, 032804 (2020).

[32] V. Guo, P. Denham, P. Musumeci, A. Ody, and Y. Park, 4D beam tomography at the UCLA Pegasus laboratory, in *Proceedings of the 12th International Beam Instrumentation Conference (IBIC'21)* (JACoW Publishing, Geneva, Switzerland, 2021), pp. 227–231.

[33] S. Jaster-Merz *et al.*, Characterization of the full transverse phase space of electron bunches at ARES, in *Proceedings of 12th International Particle Accelerator Conference (IPAC'21)* (JACoW Publishing, Geneva, Switzerland, 2021), pp. 952–955.

[34] D. Marx *et al.*, Reconstruction of the 3D charge distribution of an electron bunch using a novel variable-polarization transverse deflecting structure (TDS), J. Phys.: Conf. Ser. **874**, 012077 (2017).

[35] D. Marx *et al.*, Simulation studies for characterizing ultrashort bunches using novel polarizable X-band transverse deflection structures, Sci. Rep. **9**, 19912 (2019).

[36] D. Marx, *Characterization of Ultrashort Electron Bunches at the SINBAD-ARES Linac*, Dissertation, Universität Hamburg, Hamburg, Germany, 2019.

[37] B. Marchetti *et al.*, Experimental demonstration of novel beam characterization using a polarizable X-band transverse deflection structure, Sci. Rep. **11**, 3560 (2021).

[38] P. Craievich *et al.*, Novel X-band transverse deflection structure with variable polarization, Phys. Rev. Accel. Beams **23**, 112001 (2020).

[39] A. Grudiev, Design of compact high power RF components at X-band, CLIC Note, 2016, https://cds.cern.ch/record/2158484.

[40] P. González Caminal *et al.*, Beam-based commissioning of a novel X-band transverse deflection structure with variable polarization, Phys. Rev. Accel. Beams **27**, 032801 (2024).

[41] S. Jaster-Merz, R. W. Assmann, R. Brinkmann, F. Burkart, W. Hillert, M. Stanitzki, and T. Vinatier, 5D tomographic phase-space reconstruction of particle bunches, Phys. Rev. Accel. Beams **27**, 072801 (2024).

[42] A. Hoover, K. Ruisard, A. Aleksandrov, A. Zhukov, and S. Cousineau, Analysis of a hadron beam in five-dimensional phase space, Phys. Rev. Accel. Beams **26**, 064202 (2023).

[43] B. Cathey, S. Cousineau, A. Aleksandrov, and A. Zhukov, First six dimensional phase space measurement of an accelerator beam, Phys. Rev. Lett. **121**, 064804 (2018).

[44] H. Yutao, L. Renkai, and W. Weishi, Measurement of transverse phase space based on machine learning, High Power Laser Part. Beams **35**, 114005 (2023).

[45] A. Scheinker, A. Edelen, D. Bohler, C. Emma, and A. Lutman, Demonstration of model-independent control of the longitudinal phase space of electron beams in the linac-coherent light source with femtosecond resolution, Phys. Rev. Lett. **121**, 044801 (2018).

[46] A. Scheinker, F. W. Cropp V, and D. Filippetto, 6D phase space diagnostics based on adaptively tuned physics-informed generative convolutional neural networks, in *Proceedings of the 13th International Particle Accelerator Conference* (IPAC'22), Bangkok, Thailand (JACoW Publishing, Geneva, Switzerland, 2022), pp. 776–779.

[47] A. Scheinker, F. Cropp, and D. Filippetto, Adaptive autoencoder latent space tuning for more robust machine learning beyond the training set for six-dimensional phase space diagnostics of a time-varying ultrafast electron-diffraction compact accelerator, Phys. Rev. E **107**, 045302 (2023).

[48] R. Roussel, A. Edelen, C. Mayes, D. Ratner, J. P. Gonzalez-Aguilera, S. Kim, E. Wisniewski, and J. Power, Phase space reconstruction from accelerator beam measurements using neural networks and differentiable simulations, Phys. Rev. Lett. **130**, 145001 (2023).

[49] A. Scheinker, Physics-constrained superresolution diffusion for six-dimensional phase space diagnostics, Phys. Rev. Res. **7**, 023091 (2025).

[50] A. Scheinker, F. Cropp, S. Paiagua, and D. Filippetto, An adaptive approach to machine learning for compact particle accelerators, Sci. Rep. **11**, 19187 (2021).

[51] R. Roussel, J. P. Gonzalez-Aguilera, E. Wisniewski, A. Ody, W. Liu, J. Power, Y.-K. Kim, and A. Edelen, Efficient six-dimensional phase space reconstructions from experimental measurements using generative machine learning, Phys. Rev. Accel. Beams **27**, 094601 (2024).

[52] R. D'Arcy *et al.*, FLASHForward: Plasma wakefield accelerator science for high-average-power applications, Philos. Trans. R. Soc. A **377**, 20180392 (2019).

[53] S. Schreiber *et al.*, The free-electron laser FLASH, High Power Laser Sci. Eng. **3**, e20 (2015).

[54] W. Ackermann *et al.*, Operation of a free-electron laser from the extreme ultraviolet to the water window, Nat. Photon. **1**, 336 (2007).

[55] C. Wiebers *et al.*, Scintillating screen monitors for transverse electron beam profile diagnostics at the European XFEL, in *Proceedings of the 13th International Beam Instrumentation Conference IBIC'13* (JACoW Publishing, Geneva, Switzerland, 2013), pp. 807–810.

[56] E. Courant and H. Snyder, Theory of the alternating-gradient synchrotron, Ann. Phys. **3**, 1 (1958).

[57] A. Andersen and A. Kak, Simultaneous algebraic reconstruction technique (SART): A superior implementation of the ART algorithm, Ultrason. Imaging **6**, 81 (1984).

[58] S. van der Walt *et al.*, Scikit-image: Image processing in Python, PeerJ **2**, e453 (2014).

[59] Y. S. Derbenev, J. Rossbach, E. L. Saldin, and V. D. Shiltsev, Microbunch radiative tail-head interaction, Technical report No. TESLA-FEL 1995-05, DESY, 1995.

[60] M. Dohlus, T. Limberg, and P. Emma, Bunch compression for linac-based FEL's. Electron bunch length compression, ICFA Beam Dyn. Newslett. **38** (2006).

[61] L. Z. Rivkin, Damping ring for the SLAC linear collider, Ph.D. thesis, California Institute of Technology, 1986.

[62] E. Prat and M. Aiba, Four-dimensional transverse beam matrix measurement using the multiple-quadrupole scan technique, Phys. Rev. ST Accel. Beams **17**, 052801 (2014).

[63] M. Aicheler, P. Burrows, M. Draper, T. Garvey, P. Lebrun, K. Peach, N. Phinney, H. Schmickler, D. Schulte, and N. Toge, A multi-TeV linear collider based on CLIC technology: CLIC conceptual design report, CERN Yellow Reports: Monographs, CERN, Geneva, 2012.

[64] A. Ferran Pousa, S. Jalas, M. Kirchen, A. Martinez de la Ossa, M. Thévenet, S. Hudson, J. Larson, A. Huebl, J.-L. Vay, and R. Lehe, Bayesian optimization of laser-plasma accelerators assisted by reduced physical models, Phys. Rev. Accel. Beams **26**, 084601 (2023).

[65] P. Emma *et al.*, Bunch length measurements using a transverse RF deflecting structure in the SLAC linac, in *Proceedings of the 2nd European Particle Accelerator Conference (EPAC'02)* (JACoW Publishing, Geneva, Switzerland, 2002), pp. 1882–1884.

[66] C. Behrens *et al.*, Few-femtosecond time-resolved measurements of x-ray free-electron lasers, Nat. Commun. **5**, 3762 (2014).

[67] C. Huang, W. Lu, M. Zhou, C. E. Clayton, C. Joshi, W. B. Mori, P. Muggli, S. Deng, E. Oz, T. Katsouleas, M. J. Hogan, I. Blumenfeld, F. J. Decker, R. Ischebeck, R. H. Iverson, N. A. Kirby, and D. Walz, Hosing instability in the blow-out regime for plasma-wakefield acceleration, Phys. Rev. Lett. **99**, 255001 (2007).

[68] T. J. Mehrling, R. A. Fonseca, A. Martinez de la Ossa, and J. Vieira, Mitigation of the hose instability in plasma-wakefield accelerators, Phys. Rev. Lett. **118**, 174801 (2017).

[69] F. Burkart *et al.*, The ARES linac at DESY, in *Proceedings of the 22nd International Linear Accelerator Conference No. 31 (LINAC'22)* (JACoW Publishing, Geneva, Switzerland, 2022), pp. 691–694.

[70] A. Hoover and J. C. Wong, High-dimensional maximum-entropy phase space tomography using normalizing flows, Phys. Rev. Res. **6**, 033163 (2024).

[71] A. Hoover, *N*-dimensional maximum-entropy tomography via particle sampling, Phys. Rev. Accel. Beams **28**, L084601 (2025).